



http://pubs.acs.org/journal/acsodf Article

Hydrogen Storage in Bilayer Hexagonal Boron Nitride: A First-Principles Study

Dibya Prakash Rai,* Bhanu Chettri, Prasanta Kumar Patra, and Shahid Sattar*



Cite This: ACS Omega 2021, 6, 30362-30370



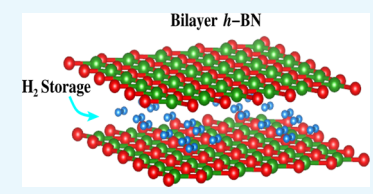
ACCESS

Metrics & More

Article Recommendations

Supporting Information

ABSTRACT: Using first-principles calculations, we report on the structural and electronic properties of bilayer hexagonal boron nitride (h-BN), incorporating hydrogen (H_2) molecules inside the cavity for potential H_2 -storage applications. Decrease in binding energies and desorption temperatures with an accompanying increase in the weight percentage (upto 4%) by increasing the H_2 molecular concentration hints at the potential applicability of this study. Moreover, we highlight the role of different density functionals in understanding the decreasing energy gaps and effective carrier masses and the underlying phenomenon for molecular



adsorption. Furthermore, energy barriers involving H_2 diffusion across minimum-energy sites are also discussed. Our findings provide significant insights into the potential of using bilayer h-BN in hydrogen-based energy-storage applications.

■ INTRODUCTION

Rising energy demands due to rapid increase in population density and depletion of natural resources is a matter of grave concern and a major threat to a sustainable future. Carbon emissions owing to the excessive burning of fossil fuels have resulted in unprecedented environmental changes in recent times, which have drastically impacted all living creatures on this planet. To tackle this, an effective and efficient approach to balance industrial developments alongside preserving natural deposits for a sustainable life is highly desirable. Therefore, enormous efforts are ongoing to capture CO₂ discharge for the purification of air, 1-3 though it is also challenging and costly. While the most effective way of capturing CO2 is fast afforestation which is hard to accomplish due to the limitations of land and rampant deforestation, use of cleaner energy resources as an alternative in factories and vehicles could partly solve issues. In this regard, proposals are underway using hydrogen (H₂) as an alternative fuel, a highly combustible gas promising for automobiles in the form of fuel cells, to tackle the global energy crisis with a minimal impact on the environment.4

Hydrogen is generated from biomass and via steam reforming of natural gas such as methane and water electrolysis which falls under fossil fuels and renewable resources. Methods such as photobiological and photochemical water splitting are under development, whereas processes such as alkaline water electrolysis, solid oxide electrolysis, and proton exchange membrane (PEM) water electrolysis are some of the established hydrogen production methods. PEM water electrolysis which contributes to around 4% of the global hydrogen production has been considered one of the most prominent techniques to generate clean and efficient hydrogen with a high production rate from renewable energy sources without any pollutants as byproducts. Moreover, biophotolysis, steam reforming, autothermal reforming, electrolysis, dark

fermentation, and so forth have been proven to have an efficiency of above 40% but lack in prospects of storage, high capital costs, transportation, and clean byproducts. Around 70 million tons per annum of hydrogen are produced around the world of which a large fraction is utilized for industrial purposes. 11,12 Because oxygen $(\mathrm{O_2})$ supports the combustion $(2\mathrm{H_2}+\mathrm{O_2} \to 2\mathrm{H_2O}+\Delta E)$, the energy derived out of burning $\mathrm{H_2}$ leads to water $(\mathrm{H_2O})$ as a natural byproduct and favors its utilization as a fuel in reducing the effects of $\mathrm{CO_2}$ emissions. Foreseeing the aforementioned prospects, a technical approach to discover potential new materials for efficient reversible $\mathrm{H_2}$ storage is much needed. 13,14

The discovery of graphene opened doors to a new era of technological revolution. $^{15-20}$ Interest in two-dimensional (2D) nanomaterials thereafter has grown exponentially finding applications in nanoscale digitization, spintronics, gas sensing, catalysis, and $\rm H_2$ production and storage, to list a few. $^{21-30}$ Due to their largest surface area-to-volume ratio and exceptional chemical stability, graphene-like materials 31,32 such as graphdiyne, 33,34 honeycomb BC $_3$, 35,36 borophene, $^{37-43}$ CN, 44,45 and g-C $_3$ N $_4$ honeycomb BCa, 35,36 borophene, investigated and recognized as a safe reservoir for $\rm H_2$ storage. Moreover, the search of potential $\rm H_2$ -storage materials in other 2D layered structures such as hexagonal boron nitride (h-BN), 28,50 boron arsenide, 51 black and blue phosphorene, $^{51-57}$ boron monochalcogenides, 58 and gallium monochalcogenides is still ongoing.

Received: June 30, 2021 Accepted: October 20, 2021 Published: November 3, 2021





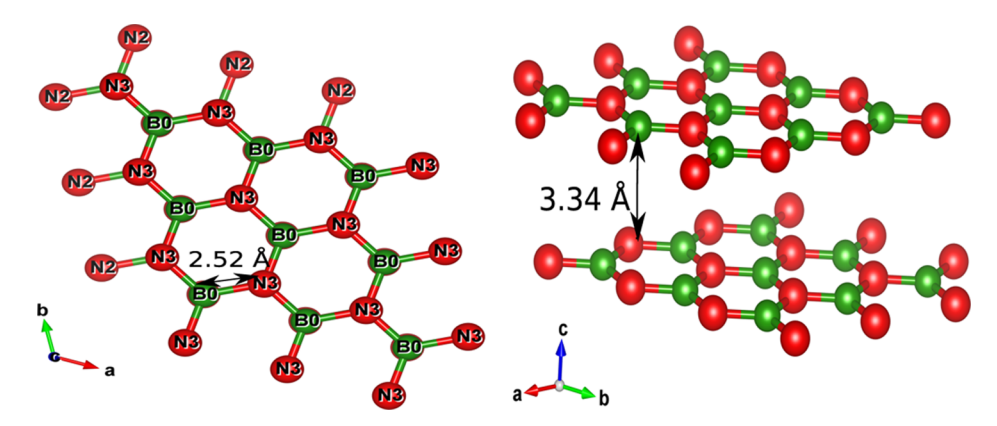


Figure 1. Top view and side view of pristine bilayer h-BN.

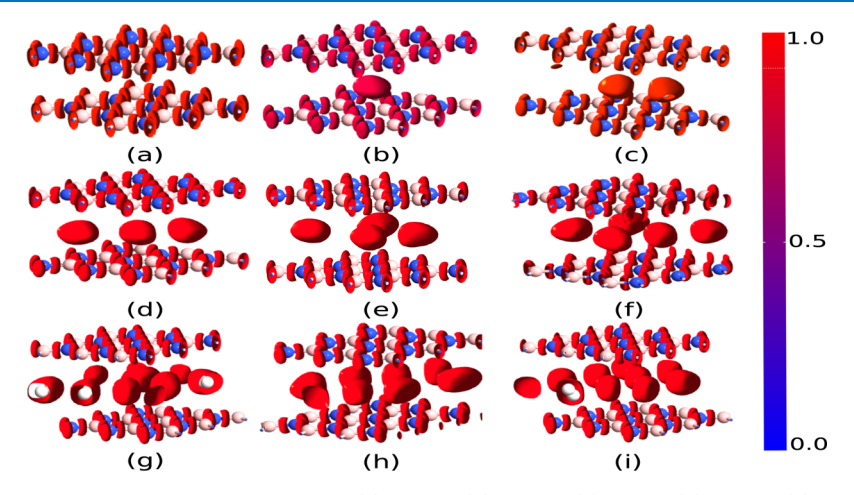


Figure 2. ELF of bilayer h-BN with the number of H_2 molecules (a) $n_H = 0$, (b) $n_H = 1$, (c) $n_H = 2$, (d) $n_H = 3$, (e) $n_H = 4$, (f) $n_H = 5$, (g) $n_H = 6$, (h) $n_H = 7$, and (i) $n_H = 8$.

H₂ gas is mostly preserved either by liquefaction under high compressing pressure 63-66 or by adsorption on the surface or interstitial region of material cavity. 67-71 In relation to this, the adsorption of H₂ on the surface of 2D materials has advantages in terms of safe functionality and cost-effectiveness. For the effective utilization of H₂ in fuel cells, the adsorption energy and gravimetric weight percentage on the adsorbent should be sufficiently high. 72,73 Recently, vehicles having H₂ fuel cells with a gravimetric weight percentage of 6% were successfully The adsorption/desorption kinetics and the strength of binding energy ought to be intermediate for hydrogen to bind on the material surfaces with an optimal adsorption energy range. Owing to the obvious reasons mentioned above and the survey of previous works, $^{75-81}$ 2D bilayer *h*-BN looks promising with numerous adequate functional properties such as high mechanical stability, carrier mobility, and outstanding electronic and optical properties which encourages its further utilization for energy-storage applications. 82-86 Motivated by this, we explore the possibility of using bilayer h-BN for H₂ storage by employing first-principles calculations. We analyzed trends in binding energy, desorption temperature, effective mass of electron and holes, and subsequently their effects on the structural and electronic properties of bilayer h-BN using state-of-the-art computational techniques.

■ COMPUTATIONAL DETAILS

Bilayer h-BN was constructed by stacking two h-BN monolayers in a AA'-stacking configuration which has been

proven to be the most stable configuration, 87,88,91 having an inplane lattice constant of $a = 2.488 \text{ Å}.^{89,90} \text{ A vacuum of } 15 \text{ Å} \text{ is}$ inserted in the out-of-plane direction to avoid spurious interactions of wave functions. We used a $3 \times 3 \times 1$ supercell consisting of 36 atoms with the B/N stoichiometric ratio of 1:1 as shown in Figure 1. The van der Waals interactions⁹¹ were incorporated using Grimme's DFT-D2 scheme. 92 The geometry of bilayer h-BN was optimized within the force field approximation using an interatomic potential developed by Stillinger Weber. 93,94 Because bilayer h-BN can accommodate eight H2 molecules between the layers at its optimal capacity, geometrical relaxations were performed for all cases after inserting H2 molecules. Moreover, the electronic properties were computed at the level of generalized gradient approximations (GGAs) of type Perdew-Burke-Ernzerhof⁹⁵ and DFT-1/2, 96,97 and a comparison has been made between both approaches. As both GGA and DFT-1/2 were treated as semilocal functionals within the framework of Kohn-Sham density functional theory (DFT), 98 self-consistency is achieved in the iterative solution for each case. A basis of the linear combination of atomic orbitals has been opted as programmed in the Quantumwise VNL-ATK package.⁹⁹ Finally, a detailed study of each system was made possible while integrating the first Brillouin zone with dense Monkhorst-Pack 16 × 16 × 1 k-mesh, ¹⁰⁰ and the k-point convergence plot is supplied in the Supporting Information. Also, for the sake of reproducibility of our work, the relaxed atomic coordinates of the h-BN bilayer

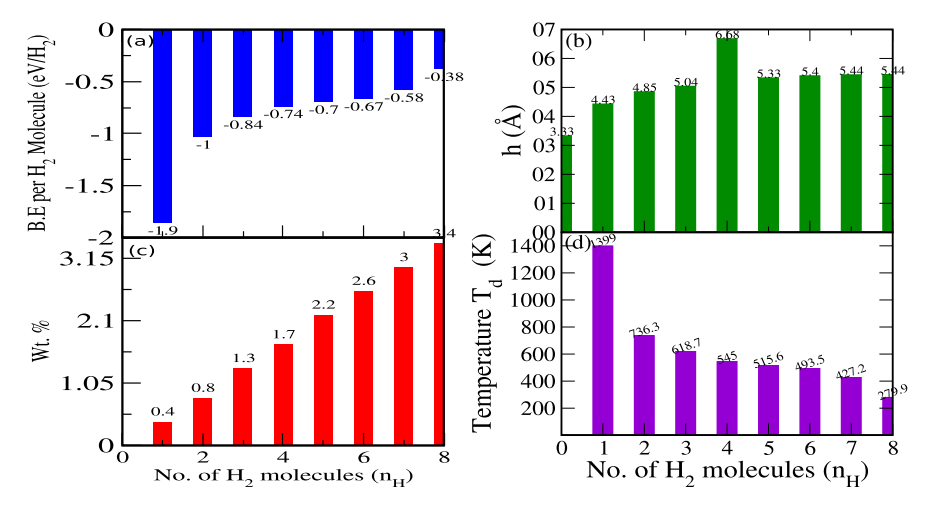


Figure 3. (a) Binding energy per H_2 molecule. (b) Interlayer spacing between adjacent h-BN monolayers. (c) Wt % with respect to H_2 content. (d) Desorption temperature (T_D) of bilayer h-BN with the number of H_2 molecules $n_H = 0$, 1, 2, 3, 4, 5, 6, 7, and 8.

and the hydrogen-adsorbed system are provided in the Supporting Information.

■ RESULTS AND DISCUSSION

The optimized in-plane lattice parameters of 2.52 Å and the interlayer spacing of 3.34 Å for the pristine bilayer h-BN are in good agreement with previous studies. 89,90,101 The ability of h-BN as a hydrogen-storage material relies on accommodating maximal number of H2 molecules while maintaining the stability (without undergoing structural deformation). In this regard, geometrical optimizations were performed by inserting H_2 molecules one after the other in the cavity of bilayer h-BN. The hollow site (in the middle of the hexagonal crystals) turns out to be the minimum-energy configuration for which atomic relaxations were performed following the Broyden-Fletcher-Goldfarb-Shanno scheme by gradually increasing the H₂ content. Figure 2a-i shows the electron localization function (ELF) of pristine and H_2 -adsorbed bilayer h-BN. The presence of electronic cloud between the B and N atoms shows the presence of intralayer covalent bonds, whereas bigger lobes around the H-H bond in between the cavity for each H₂ molecule depicts the same.

We first check the stability of our systems by computing the binding energy $(E_{\rm b})$ per ${\rm H_2}$ molecule up to maximal ${\rm H_2}$ molecular capacity by using the following definition

$$E_{\rm b} = \frac{E_{\rm T} - (E_{\rm BN} + nE_{\rm H})}{n} \tag{1}$$

where $E_{\rm T}$ is the total energy of the combined system ($h\text{-BN} + \text{H}_2$), $E_{\rm BN}$ is the total energy of the pristine bilayer h-BN, n is the number of H_2 molecules, and $E_{\rm H}$ refers to the total energy of H_2 molecules. As shown in Figure 3a, $E_{\rm b}$ remains negative even for the optimal number of H_2 molecules, which indicates stability of our systems in accommodating H_2 molecules in the bilayer h-BN cavity. Moreover, the interlayer spacing between the neighboring h-BN layers was found to be increasing with the increase of H_2 molecules (see Figure 3b). We attribute this to the expanded electronic cloud between the van der Waals gap of bilayer systems.

To provide a quantitative account of H_2 storage, we also compute dimensionless weight percentage (Wt %) for all given cases in Figure 3c using the definition of eq 2^{102}

Wt % =
$$\left[\frac{M_{\rm H}}{M_{\rm H} + M_{\rm BN}}\right] \times 100 \tag{2}$$

where $M_{\rm H}$ and $M_{\rm BN}$ are the molecular masses of the $\rm H_2$ molecule and bilayer h-BN, respectively. As expected, the Wt % increases by adding more $\rm H_2$ molecular content (see Figure 3c). Because the bilayer cavity can hold up to eight $\rm H_2$ molecules, it gives a Wt % value of 4% which is slightly less than the previously reported value of 6%. Another key aspect in this realm is to analyze the reversibility kinematics (adsorption \rightleftharpoons desorption) for which we computed the desorption temperature ($T_{\rm D}$) for all $\rm H_2$ adsorbed bilayer systems using the Van't Hoff equation given as

$$T_{\rm D}(K) = \frac{E_{\rm ads} \times R}{K_{\rm B}(\Delta S - R \ln P)}$$
(3)

where $E_{\rm ads}$ is the average adsorption energy, $R=8.3145~\rm JK^{-1}$ Mol⁻¹ is the gas constant, $K_{\rm B}=1.38\times 10^{-23}~\rm JK^{-1}$ is Boltzmann constant, ΔS represents the change in $\rm H_2$ entropy from the gas to liquid phase, and P is the equilibrium pressure taken to be 1 atm, respectively. The calculated $T_{\rm D}$ ranges from 1399 K to 279 K when increasing the number of $\rm H_2$ molecules from one to eight, as shown in Figure 3d. Our results of $T_{\rm D}$ are above the room temperature (except for 8H₂, which is just below the room temperature) up to the maximum gravimetric Wt % of 3.4%, indicating bilayer h-BN to be a potential material for storing $\rm H_2$ molecules at elevated temperatures.

We next computed one-dimensional electrostatic potential (V_E) and distribution of charge densities (n_E) in the out-of-plane direction presented in Figure 4a,b. Referring to the black

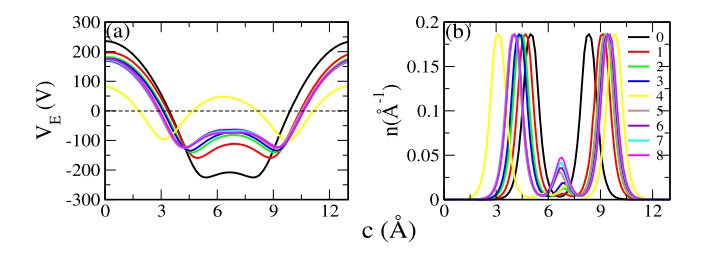


Figure 4. (a) Electrostatic potential $(V_{\rm E})$ and (b) charge density $(n_{\rm E})$ of bilayer h-BN with the number of H₂ molecules $n_{\rm H}$ = 0, 1, 2, 3, 4, 5, 6, 7, and 8.

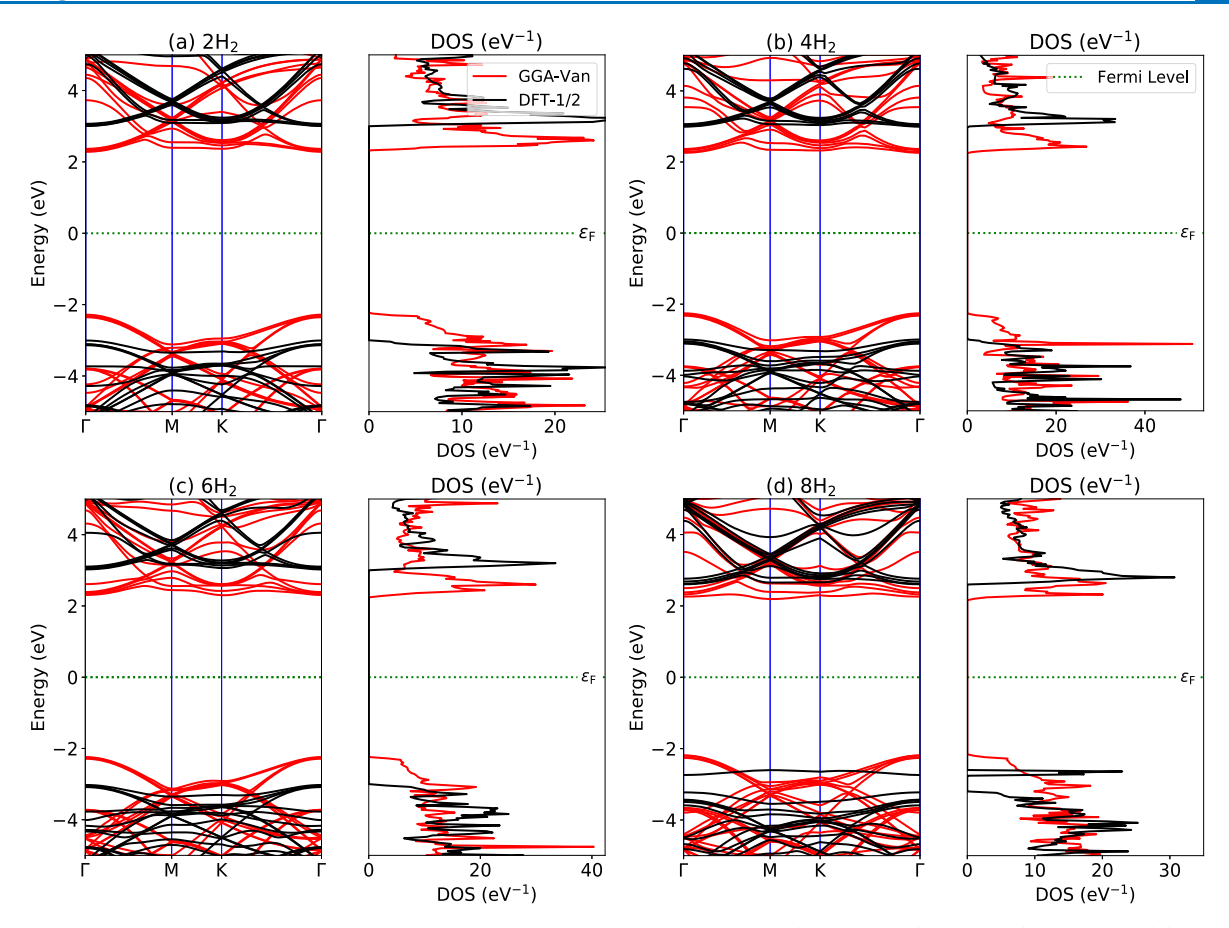


Figure 5. Electronic band structures and DOS of bilayer h-BN with number of H_2 molecules (a) $n_H = 2$, (b) $n_H = 4$, (c) $n_H = 6$, and (d) $n_H = 8$. The rest of electronic band structures and DOS are provided in the Supporting Information.

line in Figure 4a, it is noteworthy that the pristine bilayer has a flat shallow potential in between the two h-BN monolayers. However, by inserting H₂ molecules in between the bilayer cavity, the shallow peak gradually rises analogous to the case of trap electrons in a typical square well potential. The peak intensity also increases with the increase of H2 molecular concentration, except for the case of n = 4 (yellow line in Figure 4a). Here, the potential peak crosses the Fermi level $(E_{\rm F})$ giving rise to the tunneling barrier effect. The tunneling barrier (Φ) measures the efficiency of the rate of charge transfer. In the case of 4H₂, the stacking configuration is transformed from AA'- stacking configuration to AB stacking. Also, one of the H₂ molecules under structural optimization moved in the vertical direction leading to an increase in the interlayer distance to 6.8 Å. The change in the stacking configuration and the movement of a single H2 molecule close to one of the layers have led to the change in the charge distribution, thus leading to the exceptional case for n = 4. Higher value of Φ is a hindrance to the charge transfer from h- $BN \rightarrow H_2$ molecules. Following the Bader charge analysis, this can be inferred by the increase in charge density at the hydrogen site by a small amount of 0.02e, 0.017e, 0.034e, 0.021e, 0.048e, 0.055e, 0.072e, and 0.079e for $n_{\rm H}$ = 0, 1, 2, 3, 4, 5, 6, 7, and 8, respectively. Because none of the potential peaks crosses $E_{\rm F}$ except at $n_{\rm H}$ = 4, we assume Φ = 0 for all systems which allows charge transfer near the Fermi level. We can also draw similar conclusions from the one-dimensional electron density (n) plot as shown in Figure 4b. Here, the peaks in the center are due to the accumulation of charge localization of H₂

molecules whose intensity increases by the addition of $\rm H_2$ molecules. On the other side, no significant changes are observed in the charge density profiles at the B and N atomic sites. However, we notice that separation between the two peaks increases with the increase of $\rm H_2$ molecular content. We thus conclude that the increase in the number of $\rm H_2$ molecules creates a repulsive force between the two h-BN layers.

We next examine the electronic behavior of all cases (H₂ inserted bilayer h-BN) by calculating the electronic band structures and density of states (DOS) shown in Figure 5. In our previous work, we have already reported the accuracy of DFT-1/2 over GGA functionals in which an increase in band gap of $h\text{-}\mathrm{ZnSe}$ depicts consistency of results corresponding to other higher-order functionals. Referring to the band structures and DOS plots in the present situation, we again notice an increase in the band gaps in all cases within DFT-1/2 as compared to the GGA functional. Pristine bilayer h-BN exhibits an indirect band gap using both DFT-1/2 and GGA approximations along the $\Gamma \to M$ high-symmetry direction. The calculated values of the indirect band gap from DFT-1/2 and GGA approaches are 6.07 eV and 4.553 eV, respectively, for which an enhancement of \sim 33% is observed by the former. The gap thus formed is a consequence of in-plane bonding between the p-orbitals of B and N atoms correctly described by the DFT-1/2 functional. The electronic states emerge due to the presence of H-s orbitals in the energy range of 3-4 eV (see Figure 5). We compared the band gaps obtained from DFT-1/ 2 and GGA functionals with the previous results from LDA/ GGA^{86,106} and higher-order DFT-functionals^{24,107-109} and

found them in qualitative agreement. The calculated direct band gaps of the pristine and 1, 3, 5, and 7 adsorbed hydrogen molecules from GGA and DFT-1/2 are presented in the Supporting Information The values of calculated direct band gaps from GGA and DFT-1/2 are presented in Figure 6a,b.

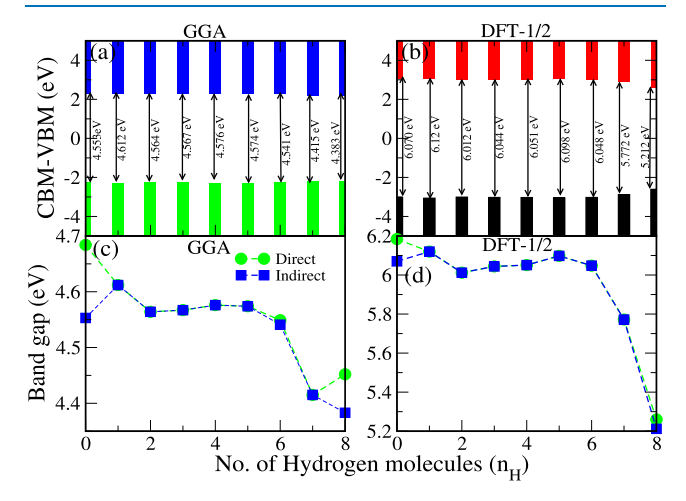


Figure 6. (a) Direct band gap using the GGA functional, (b) direct band gap using the DFT-1/2 functional, (c) direct—indirect band gap using GGA, and (d) direct—indirect band gap using DFT-1/2 of bilayer h-BN with the number of H_2 molecules $n_{\rm H} = 0$, 1, 2, 3, 4, 5, 6, 7, and 8.

Interestingly, by the insertion of H_2 molecules, we notice a transition from indirect to direct band gap for both DFT-1/2 and GGA functionals (see Figure 6a–d). However, increasing the H_2 molecular content has also reduced the band gap due to the repulsive force exerted on the B–N monolayers as discussed above (see Figure 3b).

The effective mass of holes $(m_{\rm h}^*)$ and electrons $(m_{\rm e}^*)$ is also computed with respect to the valence band maxima and conduction band minima given by eq 4¹¹⁰

$$m^* = \hbar^2 \left(\frac{\mathrm{d}^2 E}{\mathrm{d}k^2}\right)^{-1} \tag{4}$$

where E is the band energy and k refers to the wave vector of the respective charge carrier. Using both DFT-1/2 and GGA functionals, effective masses along the longitudinal (\parallel) and transverse (\perp) directions are presented in Figure 7a,b.

For the pristine bilayer h-BN, effective electron mass along \parallel and \perp directions is 2.12 m_e and 0.96 m_e , respectively, which is in reasonable agreement with the previously reported values of 2.21 $(M \to L)$ and 0.26 m_e $(M \to \Gamma)$. Similarly, the effective hole masses of 0.75 m_e (\perp) and 1.27 m_e (\parallel) are in good agreement with 0.50 m_e $(M \to \Gamma)$ and 1.33 m_e $(M \to L)$. The higher value of m_e^* is due to the presence of a flat band along the high-symmetry $M \to K$ path in the conduction band region, as shown in Figure 5a. We also compute the relative electron and hole effective mass ratio (D) using the relation $D = m_e^*/m_h^*$ and is given in Table 1 for each case.

Finally, we compute the H₂ diffusion barrier taking multiple images between the initial and final ground states by means of the nudged elastic band method as shown in Figure 8. Since hollow site is the minimum-energy configuration as discussed before, two different paths are chosen for H₂ propagation considering the bridge site (passing through the B–N bond). As can be seen in Figure 8a,b, the diffusion barrier amounts to

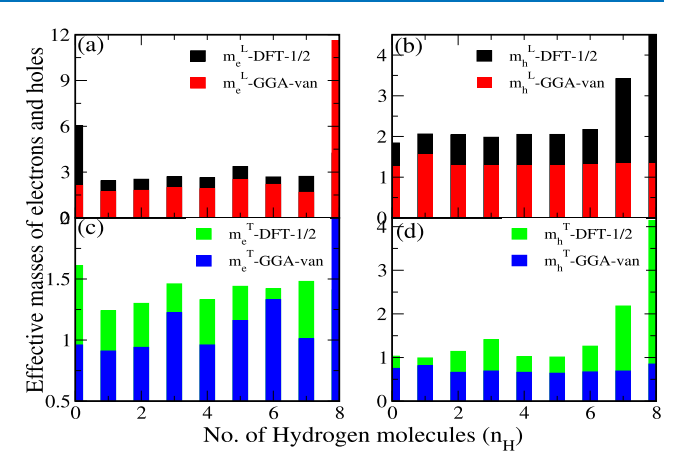


Figure 7. Using DFT-1/2 and GGA functionals, (a) electron effective mass along the longitudinal direction, (b) hole effective mass along the longitudinal direction, (c) electron effective mass along the transverse direction, and (d) hole effective mass along the transverse direction for bilayer h-BN with increasing number of H_2 molecules $n_{\rm H} = 0, 1, 2, 3, 4, 5, 6, 7,$ and 8.

Table 1. Calculated Relative Electron and Hole Effective Mass Ratios (D) Using DFT-1/2 and GGA Functionals

n_{H}	$D_{ m GGA}^{\parallel}$	$D_{ m GGA}^{\perp}$	$D_{ ext{DFT-1/2}}^{\parallel}$	$D_{ ext{DFT-1/2}}^{\perp}$
0	1.669	1.280	3.283	1.563
1	1.103	1.123	1.180	1.253
2	1.395	1.424	1.240	1.140
3	1.535	1.794	1.359	1.035
4	1.473	1.455	1.283	1.304
5	1.953	1.813	1.639	1.426
6	1.672	1.985	1.235	1.127
7	1.256	1.464	0.795	0.679
8	8.737	2.365	0.942	0.341

0.25 eV for the neighboring hexagonal site compared to 0.43 eV for the second path. For a single $\rm H_2$ with an optimized interlayer distance, the diffusion barrier amounts to 0.046 eV for the neighboring hexagonal site compared to 0.087 and 0.079 eV for the path along the bond site. Similarly, the diffusion barrier study is conducted by increasing the $\rm H_2$ molecular content in the h-BN bilayer cavity for both the reaction paths. We notice that the diffusion barrier decreases with an increase in the $\rm H_2$ molecular concentration for both the paths (see Figure 8c,d). The lower diffusion energy value signifies the higher hydrogen molecule adsorption and desorption capabilities (Table 2).

CONCLUSIONS

We presented theoretical insights into the possible use of bilayer h-BN as a potential H_2 storage medium by means of first-principles calculations. H_2 molecules energetically prefer the hollow site between the bilayer cavity for which structural relaxations indicate enlarged interlayer distances. With the insertion of optimal H_2 molecular content, negative binding energies indicate stability, whereas high desorption temperatures upto six H_2 molecules hint at a possible hindrance to reversible adsorption and desorption processes in the bilayer systems. We analyzed electronic dispersion using DFT-1/2 and GGA density functionals and found the former to correctly describe energy gaps and their nature in comparison to the latter. Moreover, effective carrier masses are calculated for each

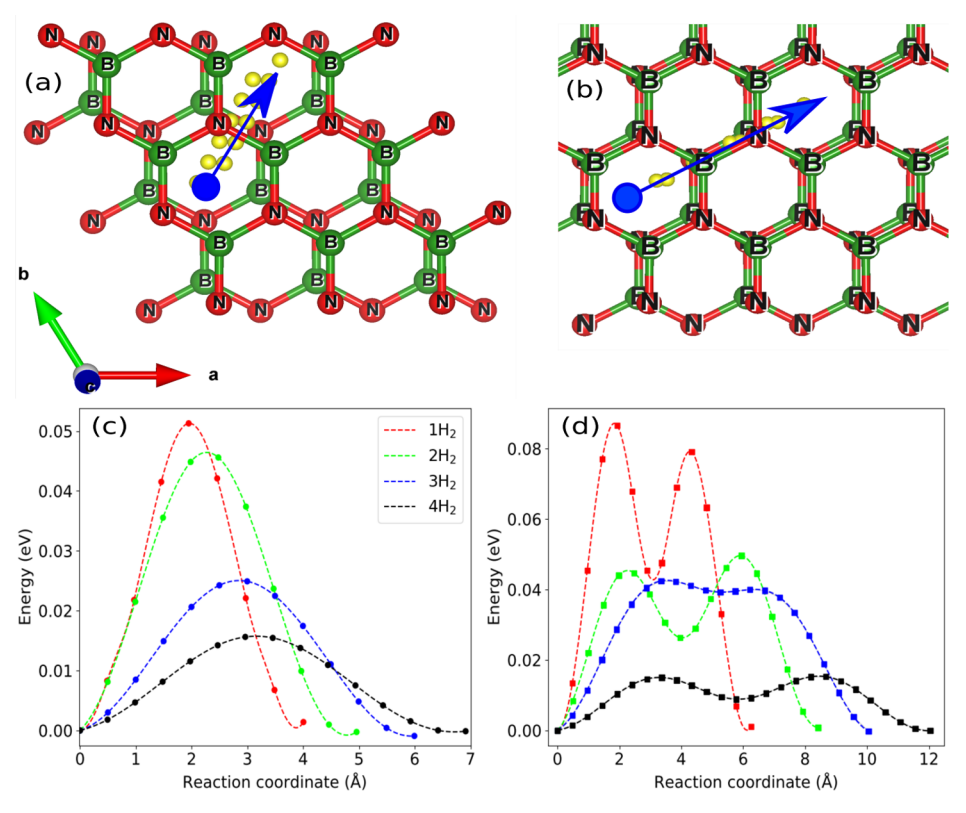


Figure 8. (Top) The reaction paths. (a) Bridge site and (b) bond site. (Bottom) Diffusion barriers with the reaction path alongside the (c) bridge site and (d) bond site with respect to the reaction coordinates.

Table 2. Diffusion Barriers for Two Different Paths, that is, Through Bridge Site and via B-N Bond Site with Different H₂ Molecular Contents

		bond site (eV)	
n_{H}	bridge site (eV)	1st peak	2nd peak
1	0.052	0.087	0.079
2	0.046	0.044	0.049
3	0.042	0.042	0.040
4	0.024	0.015	0.015

case to describe the effects of H_2 adsorption on the electron or hole transport. Finally, diffusion barriers indicate that a small energy barrier is needed for H_2 molecular propagation across the hexagonal minimum-energy sites. This comprehensive study forms the basis of further investigations (both theoretical and experimental) on potential H_2 -storage applications using bilayer h-BN cavity.

ASSOCIATED CONTENT

Supporting Information

The Supporting Information is available free of charge at https://pubs.acs.org/doi/10.1021/acsomega.1c03443.

Convergence plot of total energy with respect to the k-mesh; electronic band structures and DOS plots of bilayer h-BN adsorbed with different number of H_2 molecules; and cartesian and fractional coordinates of H_2 -adsorbed bilayer h-BN (PDF)

AUTHOR INFORMATION

Corresponding Authors

Dibya Prakash Rai — Physical Sciences Research Center (PSRC), Department of Physics, Pachhunga University College, Mizoram University, Aizawl 796001, India; orcid.org/0000-0002-3803-8923; Email: dibya@pucollege.edu.in

Shahid Sattar — Department of Physics and Electrical Engineering, Linnaeus University, Kalmar SE-39231, Sweden; ⊚ orcid.org/0000-0003-4409-0100; Email: shahid.sattar@lnu.se

Authors

Bhanu Chettri — Department of Physics, North-Eastern Hill University, Shillong 793022 Meghalaya, India; Physical Sciences Research Center (PSRC), Department of Physics, Pachhunga University College, Aizawl 796001 Mizoram, India

Prasanta Kumar Patra – Department of Physics, North-Eastern Hill University, Shillong 793022 Meghalaya, India

Complete contact information is available at: https://pubs.acs.org/10.1021/acsomega.1c03443

Notes

The authors declare no competing financial interest.

ACKNOWLEDGMENTS

D.P.R. acknowledges support from the Department of Science and Technology SERB (CRG DST-SERB, Govt. of India, New Delhi) via sanction no. CRG/2018/000009(Ver-1). S.S. thanks Carl Tryggers Stiftelsen (CTS 20:71) for the financial support.

■ REFERENCES

- (1) Özçelik, V. O.; Gong, K.; White, C. E. Highly Surface-Active Ca(OH)2 Monolayer as a CO2 Capture Material. *Nano Lett.* **2018**, 18, 1786–1793.
- (2) Gupta, K.; Singh, S.; Ramachandra Rao, M. S. Fast, reversible CO2 capture in nanostructured Brownmillerite CaFeO2.5. *Nano Energy* **2015**, *11*, 146–153.
- (3) Keith, D. W.; Holmes, G.; St. Angelo, D.; Heidel, K. A Process for Capturing CO2 from the Atmosphere. *Joule* **2018**, *2*, 1573–1594.
- (4) Staffell, I.; Scamman, D.; Velazquez Abad, A.; Balcombe, P.; Dodds, P. E.; Ekins, P.; Shah, N.; Ward, K. R. The role of hydrogen and fuel cells in the global energy system. *Energy Environ. Sci.* **2019**, 12, 463–491.
- (5) Ogden, J. Prospects for Hydrogen in the Future Energy System. Research Report—UCD-ITS-RR-18-07, 2018.
- (6) BARRETO, L.; MAKIHIRA, A.; RIAHI, K. The hydrogen economy in the 21st century: a sustainable development scenario. *Int. J. Hydrogen Energy* **2003**, 28, 267–284.
- (7) Heid, B.; Linder, M.; Orthofer, A.; Wilthaner, M. Hydrogen: the Next Wave for Electric Vehicles?. *McKinsey Cent. Future Mobil.* **2017**, 18.
- (8) Ozcanli, M.; Bas, O.; Akar, M. A.; Yildizhan, S.; Serin, H. Recent studies on hydrogen usage in Wankel SI engine. *Int. J. Hydrogen Energy* **2018**, 43, 18037–18045.
- (9) Turner, J. A. Sustainable hydrogen production. *Science* **2004**, 305, 972–974.
- (10) Young, J. L.; Steiner, M. A.; Döscher, H.; France, R. M.; Turner, J. A.; Deutsch, T. G. Direct solar-to-hydrogen conversion via inverted metamorphic multi-junction semiconductor architectures. *Nat. Energy* **2017**, *2*, 17028.
- (11) Shiva Kumar, S.; Himabindu, V. Hydrogen production by PEM water electrolysis—A review. *Mater. Sci. Energy Technol.* **2019**, *2*, 442–454.
- (12) Eljack, F.; Kazi, M.-K. Prospects and Challenges of Green Hydrogen Economy via Multi-Sector Global Symbiosis in Qatar. *Front. Sustain.* **2021**, *1*, 14.
- (13) Yu, M.; Li, S.; Falconer, J. L.; Noble, R. D. Reversible H2 storage using a SAPO-34 zeolite layer. *Microporous Mesoporous Mater.* **2008**, *110*, 579–582.
- (14) Kaczmarek, Ł.; Warga, T.; Zawadzki, P.; Makowicz, M.; Bucholc, B.; Kula, P. The influence of the hydrogenation degree on selected properties of graphene as a material for reversible H2 storage. *Int. J. Hydrogen Energy* **2019**, *44*, 23149–23159.
- (15) Novoselov, K. S.; Geim, A. K.; Morozov, S. V.; Jiang, D.; Zhang, Y.; Dubonos, S. V.; Grigorieva, I. V.; Firsov, A. A. Electric field effect in atomically thin carbon films. *science* **2004**, *306*, *666*–*669*.
- (16) Kumar, C. V.; Pattammattel, A. *Introduction to Graphene*; Elsevier, 2017, pp 1–15. DOI: 10.1016/b978-0-12-813182-4.00001-5
- (17) Gupta, A.; Sakthivel, T.; Seal, S. Recent development in 2D materials beyond graphene. *Prog. Mater. Sci.* **2015**, *73*, 44–126.
- (18) Pereira, V. M.; Guinea, F.; Lopes dos Santos, J. M. B.; Peres, N. M. R.; Castro Neto, A. H. Erratum: Disorder Induced Localized States in Graphene [Phys. Rev. Lett. 96, 036801 (2006)]. *Phys. Rev. Lett.* 2007, 98, 259902.
- (19) Niu, J.; Gao, H.; Tian, W. Synthesis and Applications of Graphene-Quantum Dot Composites. *Prog. Chem.* **2014**, *26*, 270–276
- (20) Tiwari, S. K.; Sahoo, S.; Wang, N.; Huczko, A. Graphene research and their outputs: Status and prospect. *J. Sci.: Adv. Mater. Devices* **2020**, *5*, 10–29.
- (21) Choi, K.; Lee, Y. T.; Im, S. Two-dimensional van der Waals nanosheet devices for future electronics and photonics. *Nano Today* **2016**, *11*, 626–643.
- (22) Huo, N.; Yang, Y.; Li, J. Optoelectronics based on 2D TMDs and heterostructures. J. Semicond. 2017, 38, 031002.
- (23) Garg, S.; Mollah, A. S.; Waters, J. L.; Kim, S. M.; Kung, P. Invited Transition Metal Dichalcogenide Semiconductor Growth and Large Area Devices for Optoelectronics and Sensing. *ECS Trans.* **2017**, *80*, 1–11.

- (24) Li, J.; Ding, Y.; Wei Zhang, D.; Zhou, P. Photodetectors Based on Two-Dimensional Materials and Their van der Waals Heterostructures. *Acta Phys.-Chim. Sin.* **2019**, *35*, 1058–1077.
- (25) Li, T.; He, C.; Zhang, W. Primitive and O-Functionalized R-Graphyne-like BN Sheet: Candidates for SO 2 Sensor with High Sensitivity and Selectivity at Room Temperature. *ACS Appl. Electron. Mater.* **2019**, *1*, 34–43.
- (26) Hu, W.; Yang, J. Two-dimensional van der Waals heterojunctions for functional materials and devices. *J. Mater. Chem.* C 2017, 5, 12289–12297.
- (27) Wu, H. Y.; Fan, X. F.; Kuo, J.-L.; Deng, W.-Q. Carbon doped boron nitride cages as competitive candidates for hydrogen storage materials. *Chem. Commun.* **2010**, *46*, 883–885.
- (28) Bechelany, M.; Brioude, A.; Bernard, S.; Stadelmann, P.; Cornu, D.; Miele, P. Boron nitride multiwall nanotubes decorated with BN nanosheets. *CrystEngComm* **2011**, *13*, 6526.
- (29) Shayeganfar, F.; Shahsavari, R. Oxygen- and Lithium-Doped Hybrid Boron-Nitride/Carbon Networks for Hydrogen Storage. *Langmuir* **2016**, *32*, 13313–13321.
- (30) Candini, A.; Klyatskaya, S.; Ruben, M.; Wernsdorfer, W.; Affronte, M. Graphene spintronic devices with molecular nanomagnets. *Nano Lett.* **2011**, *11*, 2634–2639.
- (31) Pasquini, L. Design of Nanomaterials for Hydrogen Storage. *Energies* **2020**, *13*, 3503.
- (32) Sattar, S.; Zhang, Y.; Schwingenschlögl, U. Stacking Effects in van der Waals Heterostructures of Silicene and Hexagonal Boron Nitride. *Adv. Theory Simul.* **2018**, *1*, 1800083.
- (33) Panigrahi, P.; Dhinakaran, A. K.; Naqvi, S. R.; Gollu, S. R.; Ahuja, R.; Hussain, T. Light metal decorated graphdiyne nanosheets for reversible hydrogen storage. *Nanotechnology* **2018**, *29*, 355401.
- (34) Zhao, W.-h.; Yuan, L.-f.; Yang, J.-l. Graphdiyne as Hydrogen Purification Membrane. *Chin. J. Chem. Phys.* **2012**, *25*, 434–440.
- (35) Zhang, Y.; Cheng, X. Hydrogen Storage on Li Coated BC 3 Honeycomb Sheet. *Chin. J. Chem.* **2017**, *35*, 1329–1332.
- (36) Zhang, H.; Liao, Y.; Yang, G.; Zhou, X. Theoretical Studies on the Electronic and Optical Properties of Honeycomb BC 3 monolayer: A Promising Candidate for Metal-free Photocatalysts. *ACS Omega* **2018**, *3*, 10517–10525.
- (37) Baraiya, B. A.; Som, N. N.; Mankad, V.; Wu, G.; Wang, J.; Jha, P. K. Nitrogen-decorated borophene: An empowering contestant for hydrogen storage. *Appl. Surf. Sci.* **2020**, *527*, 146852.
- (38) Ji, Y.; Dong, H.; Li, Y. Theoretical Predictions on Li-Decorated Borophenes as Promising Hydrogen Storage Materials. *ChemistrySelect* **2017**, *2*, 10304–10309.
- (39) Wen, T.; Xie, A.; Li, J.; Yang, Y. Novel Ti-decorated borophene χ3 as potential high-performance for hydrogen storage medium. *Int. J. Hydrogen Energy* **2020**, 45, 29059–29069.
- (40) Chen, X.; Wang, L.; Zhang, W.; Zhang, J.; Yuan, Y. Cadecorated borophene as potential candidates for hydrogen storage: A first-principle study. *Int. J. Hydrogen Energy* **2017**, *42*, 20036–20045.
- (41) Joseph, J.; Sivasankarapillai, V. S.; Nikazar, S.; Shanawaz, M. S.; Rahdar, A.; Lin, H.; Kyzas, G. Z. Borophene and Boron Fullerene Materials in Hydrogen Storage: Opportunities and Challenges. *ChemSusChem* **2020**, *13*, 3754–3765.
- (42) Wang, L.; Chen, X.; Du, H.; Yuan, Y.; Qu, H.; Zou, M. First-principles investigation on hydrogen storage performance of Li, Na and K decorated borophene. *Appl. Surf. Sci.* **2018**, 427, 1030–1037.
- (43) Liu, T.; Chen, Y.; Wang, H.; Zhang, M.; Yuan, L.; Zhang, C. Li-Decorated β 12-Borophene as Potential Candidates for Hydrogen Storage: A First-Principle Study. *Materials* **2017**, *10*, 1399.
- (44) Chen, Y.-D.; Yu, S.; Zhao, W.-H.; Li, S.-F.; Duan, X.-M. A potential material for hydrogen storage: a Li decorated graphitic-CN monolayer. *Phys. Chem. Chem. Phys.* **2018**, 20, 13473–13477.
- (45) Zhu, Y.; Wang, T.; Xu, T.; Li, Y.; Wang, C. Size effect of Pt cocatalyst on photocatalytic efficiency of g-C3N4 for hydrogen evolution. *Appl. Surf. Sci.* **2019**, *464*, 36–42.
- (46) Wang, N.; Wang, J.; Hu, J.; Lu, X.; Sun, J.; Shi, F.; Liu, Z.-H.; Lei, Z.; Jiang, R. Design of Palladium-Doped g -C 3 N 4 for Enhanced

- Photocatalytic Activity toward Hydrogen Evolution Reaction. ACS Appl. Energy Mater. 2018, 1, 2866–2873.
- (47) Bi, L.; Zhang, R.; Zhang, K.; Lin, Y.; Wang, D.; Zou, X.; Xie, T. Sulfidization of Platinum Nickel Bimetal-Decorated g-C 3 N 4 for Photocatalytic Hydrogen Production: Photogenerated Charge Behavior Study. ACS Sustainable Chem. Eng. 2019, 7, 15137—15145.
- (48) Cao, S.; Yu, J. g-C₃N₄-Based Photocatalysts for Hydrogen Generation. *J. Phys. Chem. Lett.* **2014**, *5*, 2101–2107.
- (49) Hu, W.; Yang, J. First-principles study of two-dimensional van der Waals heterojunctions. *Comput. Mater. Sci.* **2016**, *112*, 518–526.
- (50) Zhang, H.; Tong, C. J.; Zhang, Y.; Zhang, Y.-N.; Liu, L.-M. Porous BN for hydrogen generation and storage. *J. Mater. Chem. A* **2015**, *3*, 9632–9637.
- (51) Ullah, S.; Denis, P. A.; Sato, F. Hydrogenation and Fluorination of 2D Boron Phosphide and Boron Arsenide: A Density Functional Theory Investigation. *ACS Omega* **2018**, *3*, 16416–16423.
- (52) Yu, Z.; Lei, S.; Wan, N.; Luan, S.; Shen, H.; Yu, H. Effect of metal adatoms on hydrogen adsorption properties of phosphorene. *Mater. Res. Express* **2017**, *4*, 045503.
- (53) Yu, Z.; Wan, N.; Lei, S.; Yu, H. Enhanced hydrogen storage by using lithium decoration on phosphorene. *J. Appl. Phys.* **2016**, *120*, 024305.
- (54) Zhang, H.-p.; Hu, W.; Du, A.; Lu, X.; Zhang, Y.-p.; Zhou, J.; Lin, X.; Tang, Y. Doped phosphorene for hydrogen capture: A DFT study. *Appl. Surf. Sci.* **2018**, 433, 249–255.
- (55) Garara, M.; Benzidi, H.; Lakhal, M.; Louilidi, M.; Ez-Zahraouy, H.; El Kenz, A.; Hamedoun, M.; Benyoussef, A.; Kara, A.; Mounkachi, O. Phosphorene: A promising candidate for H2 storage at room temperature. *Int. I. Hydrogen Energy* **2019**, *44*, 24829–24838.
- (56) Haldar, S.; Mukherjee, S.; Ahmed, F.; Singh, C. V. A first principles study of hydrogen storage in lithium decorated defective phosphorene. *Int. J. Hydrogen Energy* **2017**, *42*, 23018–23027.
- (57) Khossossi, N.; Benhouria, Y.; Naqvi, S. R.; Panda, P. K.; Essaoudi, I.; Ainane, A.; Ahuja, R. Hydrogen storage characteristics of Li and Na decorated 2D boron phosphide. *Sustainable Energy Fuels* **2020**, *4*, 4538–4546.
- (58) Mortazavi, B.; Rabczuk, T. Boron Monochalcogenides; Stable and Strong Two-Dimensional Wide Band-Gap Semiconductors. *Energies* **2018**, *11*, 1573.
- (59) Shenoy, U. S.; Gupta, U.; Narang, D. S.; Late, D. J.; Waghmare, U. V.; Rao, C. Electronic structure and properties of layered gallium telluride. *Chem. Phys. Lett.* **2016**, *651*, 148–154.
- (60) Afaneh, T.; Fryer, A.; Xin, Y.; Hyde, R. H.; Kapuruge, N.; Gutiérrez, H. R. Large-Area Growth and Stability of Monolayer Gallium Monochalcogenides for Optoelectronic Devices. *ACS Appl. Nano Mater.* **2020**, *3*, 7879–7887.
- (61) Demirtas, M.; Ozdemir, B.; Mogulkoc, Y.; Durgun, E. Oxygenation of monolayer gallium monochalcogenides: Design of two-dimensional ternary Ga 2 X O structures (X= S, Se, Te). *Phys. Rev. B* **2020**, *101*, 075423.
- (62) Zhou, J.; Zhuang, H. L. First-Principles Study on the 1 T Phase of GaX (X=S, Se) Monolayers. *ChemistrySelect* **2016**, *1*, 5779–5783.
- (63) Cardella, U.; Decker, L.; Sundberg, J.; Klein, H. Process optimization for large-scale hydrogen liquefaction. *Int. J. Hydrogen Energy* **2017**, *42*, 12339–12354.
- (64) Hammad, A.; Dincer, I. Analysis and assessment of an advanced hydrogen liquefaction system. *Int. J. Hydrogen Energy* **2018**, 43, 1139–1151.
- (65) Cardella, U.; Decker, L.; Klein, H. Economically viable large-scale hydrogen liquefaction. *IOP Conf. Ser.: Mater. Sci. Eng.* **2017**, *171*, 012013.
- (66) Qyyum, M. A.; Chaniago, Y. D.; Ali, W.; Saulat, H.; Lee, M. Membrane-Assisted Removal of Hydrogen and Nitrogen from Synthetic Natural Gas for Energy-Efficient Liquefaction. *Energies* **2020**, *13*, 5023.
- (67) Züttel, A. Materials for hydrogen storage. *Mater. Today* **2003**, *6*, 24–33.

- (68) Thomas, K. M. Adsorption and desorption of hydrogen on metal—organic framework materials for storage applications: comparison with other nanoporous materials. *Dalton Trans.* **2009**, 1487.
- (69) Piñero, J. J.; Ramírez, P. J.; Bromley, S. T.; Illas, F.; Viñes, F.; Rodriguez, J. A. Diversity of Adsorbed Hydrogen on the TiC(001) Surface at High Coverages. *J. Phys. Chem. C* **2018**, *122*, 28013–28020.
- (70) Yu, X.; Zhang, X.; Wang, H.; Wang, Z.; Feng, G. High-Coverage H 2 Adsorption on the Reconstructed Cu 2 O(111) Surface. *J. Phys. Chem. C* **2017**, *121*, 22081–22091.
- (71) Chettri, B.; Patra, P. K.; Srivastava, S.; Lalhriatzuala; Zadeng, L.; Rai, D. P. Electronic Properties of Hydrogenated Hexagonal Boron Nitride (h-BN): DFT Study. *Senhri Journal of Multidisciplinary Studies* **2019**, *4*, 72–79.
- (72) Rivard, E.; Trudeau, M.; Zaghib, K. Hydrogen Storage for Mobility: A Review. *Materials* **2019**, *12*, 1973.
- (73) Niemann, M. U.; Srinivasan, S. S.; Phani, A. R.; Kumar, A.; Goswami, D. Y.; Stefanakos, E. K. Nanomaterials for Hydrogen Storage Applications: A Review. *J. Nanomater.* **2008**, *2008*, 1–9.
- (74) Satyapal, S.; Petrovic, J.; Read, C.; Thomas, G.; Ordaz, G. The U.S. Department of Energy's National Hydrogen Storage Project: Progress towards meeting hydrogen-powered vehicle requirements. *Catal. Today* **2007**, *120*, 246–256.
- (75) Wang, C.; Behura, S. K.; Berry, V. Temperature dependent device characteristics of graphene/h-BN/Si heterojunction. *Semicond. Sci. Technol.* **2020**, *35*, 075020.
- (76) Behera, H.; Mukhopadhyay, G. Strain-tunable band gap in graphene/h-BN hetero-bilayer. *J. Phys. Chem. Solids* **2012**, 73, 818–821.
- (77) Behzad, S. Thermal properties of biased bilayer graphene and boron nitride nanoribbons. *Phys. E* **2018**, *103*, 338–347.
- (78) Moaied, M.; Hong, J. Tuning the magnetic properties of hydrogenated bilayer graphene and graphene/h-BN heterostructures by compressive pressures. *Carbon* **2018**, *131*, 266–274.
- (79) Sakai, Y.; Saito, S. Electronic Properties of Graphene/h -BN Bilayer Superlattices. J. Phys. Soc. Jpn. 2012, 81, 103701.
- (80) Yuan, J.; Wei, Z.; Zhong, J.; Huang, Y.; Mao, Y. Point defects engineering in graphene/h-BN bilayer: A first principle study. *Appl. Surf. Sci.* **2014**, 320, 502–508.
- (81) Hao, D.; Xiaoyu, H.; Zi, Y.; Li, C.; Niu, C.; Wang, F.; Cho, J.-H.; Jia, Y. Spin-gapless and -gapped band structures of non-compensated bonding BN/Graphene bilayer. *J. Phys. D: Appl. Phys.* **2020**, 53, 505101.
- (82) Zhang, R.; Zhao, J.; Pu, J.; Lu, Z. First-Principles Investigation on the Tribological Properties of h-BN Bilayer Under Variable Load. *Tribol. Lett.* **2018**, *66*, 124.
- (83) Wang, V.; Ma, N.; Mizuseki, H.; Kawazoe, Y. First-principles study of intrinsic defect properties in hexagonal BN bilayer and monolayer. *Solid State Commun.* **2012**, *152*, 816–820.
- (84) Li, J.; Du, Y.; Mu, J.; Tian, Y.; Yin, H.; Lv, Y.; Gao, L.; Zhang, M. Structure and property study by first-principles calculations: Two-dimensional semi-hydrogenated-semi-oxidized bilayer BN (111)-oriented nanosheets. *Diamond Relat. Mater.* **2020**, 102, 107666.
- (85) Amiri, M.; Beheshtian, J.; Shayeganfar, F.; Faghihnasiri, M.; Shahsavari, R.; Ramazani, A. Electro-Optical Properties of Monolayer and Bilayer Pentagonal BN: First Principles Study. *Nanomaterials* **2020**, *10*, 440.
- (86) Gilbert, S. M.; Pham, T.; Dogan, M.; Oh, S.; Shevitski, B.; Schumm, G.; Liu, S.; Ercius, P.; Aloni, S.; Cohen, M. L.; Zettl, A. Alternative stacking sequences in hexagonal boron nitride. 2D *Materials* **2019**, *6*, 021006.
- (87) Dąbrowska, A. K.; Tokarczyk, M.; Kowalski, G.; Binder, J.; Bożek, R.; Borysiuk, J.; Stępniewski, R.; Wysmołek, A. Two stage epitaxial growth of wafer-size multilayer h-BN by metal-organic vapor phase epitaxy—a homoepitaxial approach. 2D Materials 2020, 8, 015017.
- (88) Ji, Y.; Calderon, B.; Han, Y.; Cueva, P.; Jungwirth, N. R.; Alsalman, H. A.; Hwang, J.; Fuchs, G. D.; Muller, D. A.; Spencer, M. G. Chemical vapor deposition growth of large single-crystal mono-,

- bi-, tri-layer hexagonal boron nitride and their interlayer stacking. ACS Nano 2017, 11, 12057–12066.
- (89) Hummel, F.; Gruber, T.; Grüneis, A. A many-electron perturbation theory study of the hexagonal boron nitride bilayer system*. Eur. Phys. J. B 2016, 89, 235.
- (90) Constantinescu, G.; Kuc, A.; Heine, T. Stacking in Bulk and Bilayer Hexagonal Boron Nitride. *Phys. Rev. Lett.* **2013**, *111*, 036104.
- (91) Hsing, C.-R.; Cheng, C.; Chou, J.-P.; Chang, C.-M.; Wei, C.-M. Van der Waals interaction in a boron nitride bilayer. *New J. Phys.* **2014**, *16*, 113015.
- (92) Grimme, S.; Antony, J.; Ehrlich, S.; Krieg, H. A consistent and accurate ab initio parametrization of density functional dispersion correction (DFT-D) for the 94 elements H-Pu. *J. Chem. Phys.* **2010**, 132, 154104.
- (93) Zhou, X. W.; Ward, D. K.; Martin, J. E.; van Swol, F. B.; Cruz-Campa, J. L.; Zubia, D. Stillinger-Weber potential for the II-VI elements Zn-Cd-Hg-S-Se-Te. *Phys. Rev. B: Condens. Matter Mater. Phys.* **2013**, 88, 085309.
- (94) Schneider, J.; Hamaekers, J.; Chill, S. T.; Smidstrup, S.; Bulin, J.; Thesen, R.; Blom, A.; Stokbro, K. ATK-ForceField: a new generation molecular dynamics software package. *Modell. Simul. Mater. Sci. Eng.* **2017**, *25*, 085007.
- (95) Perdew, J. P.; Burke, K.; Ernzerhof, M. Generalized Gradient Approximation Made Simple [Phys. Rev. Lett. 77. Phys. Rev. Lett. 1996, 77, 3865–3868.
- (96) Ferreira, L. G.; Marques, M.; Teles, L. K. Slater half-occupation technique revisited: the LDA-1/2 and GGA-1/2 approaches for atomic ionization energies and band gaps in semiconductors. *AIP Adv.* **2011**, *1*, 032119.
- (97) Ferreira, L. G.; Marques, M.; Teles, L. K. Approximation to density functional theory for the calculation of band gaps of semiconductors. *Phys. Rev. B: Condens. Matter Mater. Phys.* **2008**, 78, 125116.
- (98) Kohn, W.; Sham, L. J. Self-Consistent Equations Including Exchange and Correlation Effects. *Phys. Rev.* **1965**, *140*, A1133–A1138.
- (99) Smidstrup, S.; Stradi, D.; Wellendorff, J.; Khomyakov, P. A.; Vej-Hansen, U. G.; Lee, M.-E.; Ghosh, T.; Jónsson, E.; Jónsson, H.; Stokbro, K. First-principles Green's-function method for surface calculations: A pseudopotential localized basis set approach. *Phys. Rev. B* **2017**, *96*, 195309.
- (100) Monkhorst, H. J.; Pack, J. D. Special points for Brillouin-zone integrations. *Phys. Rev. B: Condens. Matter Mater. Phys.* **1976**, 13, 5188–5192.
- (101) Hod, O. Graphite and Hexagonal Boron-Nitride have the Same Interlayer Distance. Why? *J. Chem. Theory Comput.* **2012**, 8, 1360–1369.
- (102) Kumar, A.; Vyas, N.; Ojha, A. K. Hydrogen storage in magnesium decorated boron clusters (Mg2Bn, n = 4–14): A density functional theory study. *Int. J. Hydrogen Energy* **2020**, 45, 12961–12971.
- (103) Tavhare, P.; Titus, E.; Chaudhari, A. Boron substitution effect on adsorption of H2 molecules on organometallic complexes. *Int. J. Hydrogen Energy* **2019**, *44*, 345–353.
- (104) Chakraborty, B.; Ray, P.; Garg, N.; Banerjee, S. High capacity reversible hydrogen storage in titanium doped 2D carbon allotrope Ψ-graphene: Density Functional Theory investigations. *Int. J. Hydrogen Energy* **2020**, *46*, 4154–4167.
- (105) Rai, D.; Laref, A.; Khuili, M.; Al-Qaisi, S.; Vu, T. V.; Vo, D. D. Electronic, magnetic and optical properties of monolayer (ML) hexagonal ZnSe on vacancy defects at Zn sites from DFT-1/2 approach. *Vacuum* **2020**, *182*, 109597.
- (106) Tang, Y. R.; Zhang, Y.; Cao, J. X. Modulating the band gap of a boron nitride bilayer with an external electric field for photocatalyst. *J. Appl. Phys.* **2016**, *119*, 195303.
- (107) Ashhadi, M.; Ketabi, S. A. Quasi-particle energies and excitonic effects in bilayer of hexagonal boron nitride. *Solid State Commun.* **2014**, *187*, 1–4.

- (108) Topsakal, M.; Aktürk, E.; Ciraci, S. First-principles study of two- and one-dimensional honeycomb structures of boron nitride. *Phys. Rev. B: Condens. Matter Mater. Phys.* **2009**, *79*, 115442.
- (109) Goriachko, A.; He, Y.; Knapp, M.; Over, H.; Corso, M.; Brugger, T.; Berner, S.; Osterwalder, J.; Greber, T. Self-assembly of a hexagonal boron nitride nanomesh on Ru(0001). *Langmuir* **2007**, 23, 2928–2931.
- (110) Bhattarai, R.; Shen, X. Predicting a Novel Phase of 2D SiTe2. *ACS Omega* **2020**, *5*, 16848–16855.
- (111) Xu, Y. N.; Ching, W. Y. Calculation of ground-state and optical properties of boron nitrides in the hexagonal, cubic, and wurtzite structures. *Phys. Rev. B: Condens. Matter Mater. Phys.* **1991**, 44, 7787–7798.